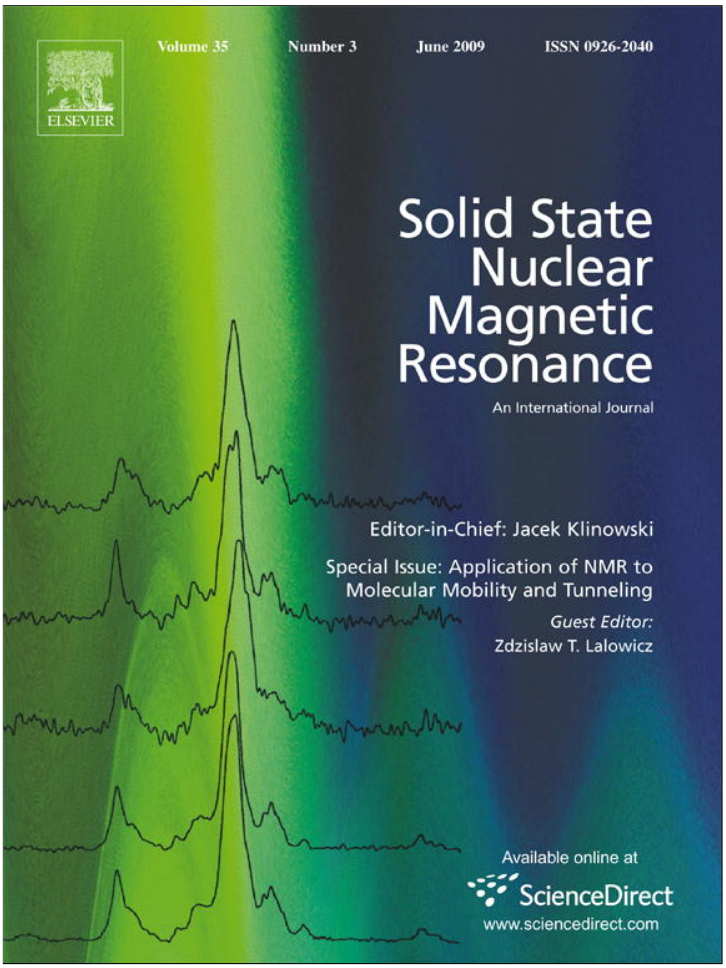

Solid State Nuclear Magnetic Resonance 35 (2009) 164–171

Contents lists available at ScienceDirect

Solid State Nuclear Magnetic Resonance

journal homepage: www.elsevier.com/locate/ssnmr

^{2}H-solid-state-NMR study of hydrogen adsorbed on catalytically active ruthenium coated mesoporous silica materials

Bernadeta Walaszek [a], Xu Yeping [a], Anna Adamczyk [b], Hergen Breitzke [b], Katrin Pelzer [c], Hans-Heinrich Limbach [a], Jianlin Huang [d], Hexing Li [d], Gerd Buntkowsky [e,*]

[a] Institut für Physikalische und Theoretische Chemie, Freie Universität Berlin, Takustr.3, D-14195 Berlin, Germany
[b] Institut für Physikalische Chemie, Friedrich Schiller Universität Jena, Helmholtzweg 4, D-07743 Jena, Germany
[c] Fritz-Haber-Institut der Max-Planck-Gesellschaft, Department for Inorganic Chemistry, Faradayweg 4-6, D-14195 Berlin, Germany
[d] Shanghai Normal University, Department of Chemistry, Shanghai 200234, PR China
[e] Institute of Physical Chemistry III, Darmstadt University of Technology, D-64287 Darmstadt, Germany

ARTICLE INFO

Article history:
Received 6 January 2009
Received in revised form
17 February 2009
Available online 13 March 2009

Keywords:
Silica
Ruthenium
Immobilized catalysts
Deuteron NMR

ABSTRACT

^{2}H solid-state NMR measurements were performed on three samples of ruthenium nanoparticles synthesized inside two different kinds of mesoporous silica, namely SBA-3 silica materials and SBA-15 functionalized with –COOH groups and loaded with deuterium gas. The line-shape analyses of the spectra reveal the different deuteron species. In all samples a strong –OD signal is found, which shows the catalytic activity of the metal, which activates the D–D bond and deuterates the –SiOH groups through the gas phase, corroborating their usability as catalysts for hydrogenation reactions. At room temperature the mobility of the –Si–OD groups depends on the sample preparation. In addition to the –Si–OD deuterons, the presence of different types of deuterons bound to the metal is revealed. The singly coordinated –Ru–D species exhibit several different quadrupolar couplings, which indicate the presence of several non-equivalent binding sites with differing binding strength. In addition to the dissociated hydrogen species there is also a dihydrogen species –Ru–D_2, which is attributed to defect sites on the surface. It exhibits a fast rotational dynamics at all temperatures. Finally there are also indications of three-fold coordinated surface deuterons and octahedrally coordinated deuterons inside the metal.

1. Introduction

Organometallic catalysts are widely used in organic synthesis, as for example in pharmaceutical and natural products chemistry and fine synthesis. Owing to the favorable properties of heterogeneous catalysts many attempts of the production of catalytic active organic–inorganic hybrid materials were done in recent years [1–23]. In these so called immobilized catalysts, the organic or organometallic functional groups are immobilized on a solid inorganic support by binding for example to the outer surface of nanoparticles or the inner surfaces of micro- or mesoporous materials. Depending on the intended application, the functional group is immobilized on the surface by various techniques [24–26]. Recent examples of immobilized catalysts contain metals such as Zn, Cu, Ru, Rh and Pt [27]. While the separation of the catalyst from the reactants is always a problem in a homogeneous reaction, immobilized catalysts can be very easily separated and reused. Furthermore, by using immobilized catalysts, less heavy metal is employed, which is in agreement with the principles of green chemistry [27].

Since the pore structure of the support material prevents the swelling or aggregation of the active site of the catalysts on the large inner surface, the active surface area of the catalyst can be increased dramatically. As a result, the efficiency of the catalyst can be enhanced by immobilization the active part of a homogeneous catalyst into mesoporous materials [20,27].

In a set of recent papers we have shown that variable temperature ^{2}H solid-state NMR line-shape analysis is a powerful technique for the characterization of the binding of hydrogen/deuterium to transition metal atoms and clusters [28–34]. The characteristic values of quadrupolar coupling constants and asymmetry parameters can be attributed to particular deuterium–ruthenium bonding situations and deuterons exhibit a tremendous amount of dynamics adsorbed on metal nanoparticles [32,35].

In our previous studies we focused on molecular complexes and well-defined magic-cluster nanoparticles. In the present

* Corresponding author. Fax: +49 6151 164347.
E-mail addresses: gerd.buntkowsky@chemie.tu-darmstadt.de, gerd.buntkowsky@uni-jena.de (G. Buntkowsky).

0926-2040/$ - see front matter © 2009 Elsevier Inc. All rights reserved.
doi:10.1016/j.ssnmr.2009.02.006

paper we apply this technique to the study of deuterium interaction with metallic ruthenium stabilized by mesoporous silica. These materials have the advantage of combining the large inner surfaces with the high catalytic activities of the transition metal.

Ordered mesoporous silica materials were discovered in 1992, when the M41S family of mesoporous silica materials was developed by the researchers of Mobil [36]. Starting with this seminal discovery, ordered mesoporous silica materials became one of the hot topics in material science, mainly because of their outstanding application potentials in heterogeneous catalysis [37], drug delivery [38] and many other fields [39]. Their adjustable pore diameters are usually in the range of 20–500 Å. Due to the high density of the pores and relatively small pore diameters, mesoporous systems possess extremely large inner surface, as compared to the volume of the individual particles. Mesoporous silica are usually synthesized by hydrolysis of Tetraethyl orthosilicate (TEOS) with structure-directing agents, [40] for instance, ionic surfactant CTMABr for MCM-41 [36], $C_{12}H_{25}(C_2H_4O)_8$ for HMS [41], and triblock copolymer for SBA-15 [42] or polyglycerol [43]. The pore sizes of these templated silicas are all ordered within certain narrow ranges.

Their catalytic applicability can be enhanced by chemical modification of the surfaces. The first example of chemical modification is the incorporation of transition metals in the pores [44]. Moreover, the pore surface can be functionalized with many functional groups and the outer surface can be selectively modified [45,46]. Since an efficient catalyst necessitates efficient transport channels to and from the active spots on the inner surface of the pores, the study of transport processes and host/guest interactions in the pores is of high importance [47,48].

In particular for hydrogenation reactions the study of the mobility and bonding situation of hydrogen/deuterium ligands on the surface of the nanoparticles stabilized by mesoporous systems is essential.

With the support from mesoporous silica, Ru particle can disperse almost homogeneously on silica surface. Ru/SiO_2 can be a good catalyst for hydrogenation, for instance, hydrogenation of unsaturated aldehyde [49], and Fischer–Tropsch synthesis [50].

The rest of this paper is organized as follows: First, the basics of ^{2}H-NMR line-shape theory are briefly summarized. Then, short introduction into the D–Ru bonding situations and their characteristic Q_{cc} and η is given. Next, the syntheses of the nanoparticles inside the silica materials are presented. The experimental section shortly introduces our home build three channel NMR spectrometer. At last, the experimental low-temperature ^{2}H-NMR studies of three different samples of ruthenium nanoparticles are presented, discussed, and summarized.

2. Materials and methods

2.1. Synthesis of mesoporous silica SBA-3

The mesoporous SBA-3 material, which is used as supporting and protective material for the catalytic ruthenium nanoparticles is prepared in strong acidic solution with CTMABr followed by removal of surfactant by calcinations. According to BJH calculations the pore size distribution is centered close to 4 nm [51].

2.2. Sample preparation

Three different samples were prepared, two with neat SBA-3 as host and one with functionalized SBA-15 as host.

Sample 1 consists of ruthenium nanoparticles embedded in neat SBA-3. The Ru/SiO_2 nanoparticles were synthesized by the reduction of $RuCl_3$/silica with $NaBH_4$. 2 g of dried silica (SBA-3) was added into the 100 ml solution containing of 1.2 g of $RuCl_3$ and 0.1 ml of HCl. After 2 days, the mixture was heated in an oven at 50 °C to evaporate the water. Then, it was dried and the $RuCl_3/SiO_2$ was heated to 180 °C in an oven for 24 h. The resulting mixture was reduced by 80 ml of KBH_4 solution, including 2.35 g of KBH_4 and 1.05 g of NaOH. After the reduction, Ru/SiO_2 was washed many times by ethanol and distilled water until it became neutral (controlled by pH paper). The Ru/SiO_2 was preserved in ethanol, in order to protect it from the oxidation by air. Before the NMR measurement, the ethanol was removed with a vacuum line with heating at 50 °C, followed by adsorption of deuterium gas at room temperature at an initial pressure of 800–900 mbar. After adsorption the excess deuterium was removed by evacuation again and the sample was flame sealed in a 5 mm glass NMR tube.

Sample 2 consists also of ruthenium nanoparticles embedded in neat SBA-3. Since sample 1 was prepared with the help of an ethanol solution there are –CD groups present in the sample, as is shown below in the results section. To be able to study a –CD free sample, sample 2 was prepared in an ethanol free synthesis, which is slightly different from the way of preparation of sample 1. The Ru/SiO_2 nanoparticles were synthesized by the reduction of $RuCl_3$/silica with H_2 gas.$RuCl_3$ of (0.60 g) was impregnated into 1 g of dried silica with HCl in a similar procedure as described above. The resulting $RuCl_3/SiO_2$ was reduced for 4 h by H_2 gas at 420 °C in a tubular oven with continuous H_2 gas flow. The outgoing gas was washed by 100 ml distilled water. The occurrence of the reduction was proved by measuring the pH value of the absorption water with pH paper ($pH < 2$) at the end. Then, it was placed in a 5 mm NMR tube, evacuated, treated with the D_2 gas for 2 h, evacuated again, and flame sealed.

Sample 3, which contains ruthenium nanoparticles embedded in SBA-15 silica functionalized with –COOH groups was prepared as follows. First, the surface of the neat silica was cleaned on a vacuum line at 180 °C. Then, a solvent with 200 mg/10 mL of Ru(COD)(COT)/THF was added to 150 mg of porous solid. After 24 h the solution was dried and the precursor inside the pores was decomposed by 3 bar of H_2 gas (24 h). The color of the porous material changes from white to black, showing the formation of the metal nanoparticles. The resulting powder was filtrated and stored under vacuum for 24 h [52]. Next it was placed in a 5 mm glass NMR tube under argon atmosphere, evacuated on a vacuum line, treated with D_2 gas for 2 h, evacuated again and flame sealed.

2.3. ^{2}H solid-state NMR

The basic theory of solid-state ^{2}H-NMR is well-documented [53] and only briefly summarized here.

The leading interaction in ^{2}H solid-state NMR is the quadrupolar interaction. In high field approximation the quadrupolar Hamiltonian of a spin 1 nucleus is given by

$$\widehat{H}_Q = 2\pi\upsilon_Q(\vartheta,\varphi)(\widehat{I}_Z^2 - \tfrac{2}{3}), \tag{1}$$

where $\widehat{I}_z$ is the angular momentum operator in the z-direction. The orientation dependent quadrupolar shift ν_Q is given by

$$\upsilon_Q(\vartheta,\varphi) = \pm Q_{zz}\tfrac{1}{2}(3\cos^2\vartheta - 1 - \eta\sin^2\vartheta\cos 2\varphi) \tag{2}$$

In Eq. (2) eQ is a quadrupole moment, eq represents the principal component of the EFG tensor, η is the asymmetry parameter, which gives information about the shape of the electric field gradient, and Q_{zz} is a measure for the strength of the quadrupolar interaction; ϑ and φ are the azimuthal and polar angles of the quadrupolar PAS with respect to the external magnetic field B_0.

In a non-oriented powder sample the average over all possible orientations has to be calculated by integration over the polar angles ϑ and φ. The quadrupolar coupling Q_{cc} constant is obtained from the experiment as

$$Q_{cc} = \frac{4}{3} Q_{zz} = \frac{e^2 qQ}{h} \quad (3)$$

2.4. Spectrometer and data evaluation

All experiments were performed at a field of 7.03 T corresponding to a ^{2}H resonance frequency of 46.03 MHz. An Oxford wide bore magnet (89 mm) equipped with a room temperature shim unit was used. The home-build three channel spectrometer has been described recently by some of us [54,55].

For the experiments a home-build 5 mm ^{2}H-NMR probe was used [29,30]. Low-temperature measurements were performed in a dynamic Oxford CF1200 helium flow cryostat. An Oxford ITC 503 temperature controller was used to control the temperature. The typical 90° pulse width was 4.5 μs. Solid echo technique with an echo spacing of 30 μs was used. The repetition time of the experiments was chosen between 1 and 10 s, depending on the T_1 relaxation time of the samples. Apodiziation of the spectra was performed by multiplication with a Hanning window and a decaying exponential with a time constant of 230 μs (1.4 kHz line broadening). To acquire the deuterium powder patterns in these samples with reasonable signal-to-noise ratio, nearly 2000 scans per spectrum were accumulated.

The laboratory written Matlab programs used in spectra evaluation are based on the theory of solid-state ^{2}H-NMR and described elsewhere [56–58].

3. Results and discussion

The electric field gradient tensor, which determines the quadrupolar interaction, depends on the mobility of measured quadrupolar atoms. Changes of this tensor induce changes of the line-shape, thus the changes of the quadrupolar coupling constants. In molecular complexes these changes were introduced by the exchange motions of the deuterium ligands. At very low temperatures the exchange motions of most systems are frozen and the real value of the quadrupolar interaction is determined. At higher temperatures or for very low exchange potentials only apparent quadrupolar interactions with reduced interaction strength are found. Nevertheless, the reductions of the Q_{cc} values are characteristic of specified bonding situations.

In a set of recent papers we have characterized the quadrupolar interactions, characteristic of specific binding situations of the deuterons to transition metal complexes and surfaces. Details about mononuclear complexes are found in Ref. [34]. Studies of polynuclear complexes will be published elsewhere [59].

3.1. ^{2}H solid-state NMR studies of sample 1

In this sample the ruthenium metal is amorphous, does not exhibit XRD diffraction peaks and is characterized by a relatively large active specific surface. The dark area in the TEM micrographs (see Fig. 1) displays the nanoparticles, filling the pores of SBA-3 (pore diameters of 3.8 nm). The length of the metal nanoparticles filling the inside of the pores is typically longer than 10 nm.

The ^{2}H solid-state experiments were performed in the temperature range of 100–300 K. The resulting spectra and their simulation and deconvolution into sub-spectra are presented in Fig. 2 (see also Table 1).

The room temperature spectrum consists of five Pake-like subspectra and a weak narrow central line. The experimental values of the quadrupolar interaction for the five sub-spectra are as follows: $Q_{zz1} = 160$ kHz; $Q_{zz2} = 90$ kHz; $Q_{zz3} = 52$ kHz; $Q_{zz4} = 30$ kHz; and $Q_{zz5} = 14$ kHz. A similar situation is found at 250 K, where the quadrupolar tensor values are given by: $Q_{zz1} = 160$ kHz; $Q_{zz2} = 90$ kHz; $Q_{zz3} = 54$ kHz; $Q_{zz4} = 34$ kHz; and $Q_{zz5} = 16$ kHz. The major intensity is in the broad component. A similar situation is found in the spectrum measured at 150 K. The quadrupolar tensor values are as follows: $Q_{zz1} = 180$ kHz; $Q_{zz2} = 90$ kHz; $Q_{zz3} = 54$ kHz; $Q_{zz4} = 38$ kHz; and $Q_{zz5} = 20$ kHz. At the lowest measured temperature (100 K) the spectrum consists of four Pake-like sub-spectra. The narrow line disappears and the major intensity is in the component of $Q_{zz1} = 180$ kHz. The remaining three signals with very low intensities have the quadrupolar tensor values of $Q_{zz2} = 90$ kHz; $Q_{zz3} = 54$ kHz; $Q_{zz4} = 38$ kHz.

The broad component of 160–180 kHz can be attributed to the O–D groups from the deuterated silanol (Si–OD) groups. Their deuteration is a clear indication of the catalytic activity of the ruthenium nanoparticles (see discussion below). Moreover, their mobility is reduced as compared to sample 2 and 3 (see below).

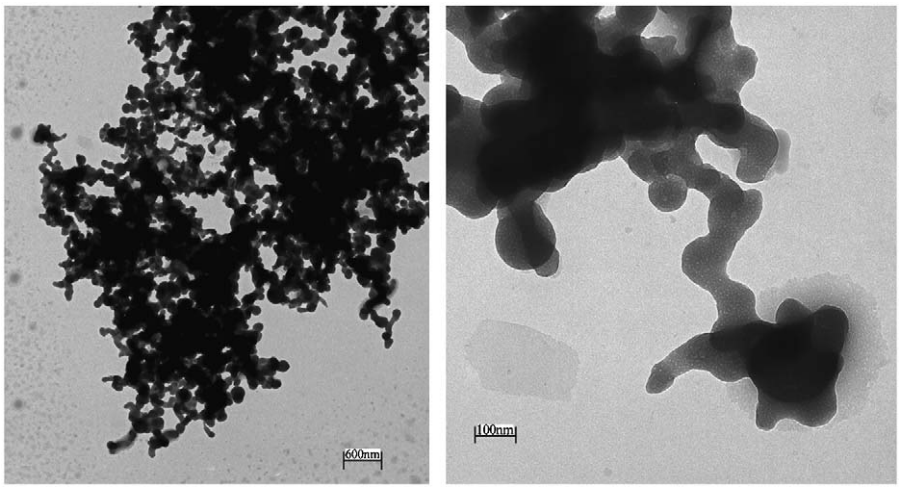

Fig. 1. TEM micrograph of ruthenium nanoparticles inside the SBA-3 silica.

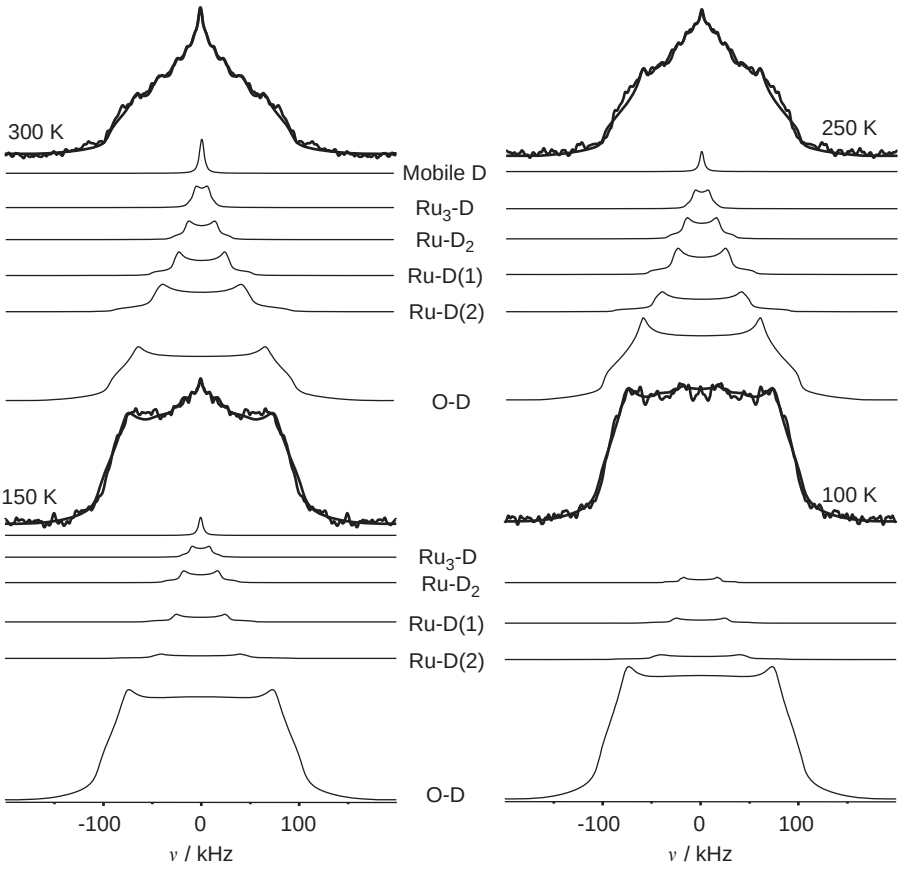

Fig. 2. Solid-state 46.03 MHz ^{2}H-NMR spectra of sample 1. The experimental spectra are simulated by the sum of the corresponding sub-spectra (see Table 1 and text).

Table 1
Parameters found by the line-shape analysis of ^{2}H-NMR spectra of sample 1 (i.e. Q_{zz}, η, intensities, and the assignments of the signals).

T (K)	Signals	Intensities	$Q_{zz} \pm 5$ (kHz)	$\eta \pm 0.01$	Assignments
300	Q_{zz1}	4.53×10^9	160	0.18	OD
	Q_{zz2}	1.12×10^9	90	0.10	RuD(2)
	Q_{zz3}	5.09×10^8	52	0.10	RuD(1)
	Q_{zz4}	2.77×10^8	30	0.10	RuD_2
	Q_{zz5}	1.89×10^8	14	0.10	Surface deuterium and/or Ru_3–D
250	Q_{zz1}	6.52×10^9	160	0.25	OD
	Q_{zz2}	7.19×10^8	90	0.10	RuD(2)
	Q_{zz3}	6.07×10^8	54	0.10	RuD(1)
	Q_{zz4}	3.43×10^8	34	0.10	RuD_2
	Q_{zz5}	1.8×10^8	16	0.10	Surface deuterium and/or Ru_3–D
150	Q_{zz1}	6.35×10^9	180	0.16	OD
	Q_{zz2}	8.52×10^7	90	0.10	RuD(2)
	Q_{zz3}	8.73×10^7	54	0.08	RuD(1)
	Q_{zz4}	1.02×10^8	38	0.10	RuD_2
	Q_{zz5}	6.18×10^7	20	0.06	Surface deuterium and/or Ru_3–D
100	Q_{zz1}	7.11×109	180	0.16	OD
	Q_{zz2}	9.01×107	90	0.10	RuD(2)
	Q_{zz3}	5.42×107	54	0.08	RuD(1)
	Q_{zz4}	3.38×107	38	0.10	RuD_2

In model complexes a value of $Q_{zz} = 70$ kHz was found for deuterons bound on top of a single Ru-metal atom. By comparison the signals at 54 and 90 kHz can be attributed to D ligands bounded on top of the ruthenium atom. Since the quadrupolar interaction depends on the bond distance between the interacting atoms [60], the variation of the quadrupolar interaction is an indication of the existence of different on top sites for deuterons with different binding strength.

The weak signal of 30–40 kHz coincides with the signal of D_2 ligands rotating about the Ru–D_2 axis, which causes a reduction of the quadrupolar tensor [34]. Thus this signal is tentatively attributed to Ru–D_2 ligands (see discussion below). The component of 16–20 kHz can be attributed to deuterium atoms coordinated to three ruthenium atoms on the surface [59].

The existence of these different binding sites can be understood by taking the amorphous nature of the metal inside the pores into account.

3.2. ^{2}H solid-state NMR studies of sample 2

The temperature range of the measurements of this sample was between 25 and 300 K (see Fig. 3, Table 2). The room temperature spectrum consists of four Pake-like sub-spectra and the narrow line, in the center. The quadrupolar tensor values are equal to $Q_{zz1} = 180$ kHz; $Q_{zz2} = 70$ kHz; $Q_{zz3} = 30$ kHz; $Q_{zz4} = 14$ kHz. The major intensity is distributed over the narrow central line and the Q_{zz1}-Pake signal. In the spectrum measured at 120 K the major intensity is in the component of $Q_{zz1} = 188$ kHz. Three other quadrupolar tensor values are as follows: $Q_{zz2} = 70$ kHz; $Q_{zz3} = 40$ kHz; $Q_{zz4} = 18$ kHz. The spectrum at 50 K can be again decomposed into four Pake-like sub-spectra with the quadrupolar interactions characterized by: $Q_{zz1} = 200$ kHz; $Q_{zz2} = 80$ kHz; $Q_{zz3} = 45$ kHz; $Q_{zz4} = 18$ kHz. At 25 K the spectrum consists of four Pake-like sub-spectra with the major intensity in the component of $Q_{zz1} = 200$ kHz; moreover, the narrow central line is still seen. Three remaining components can be characterized by

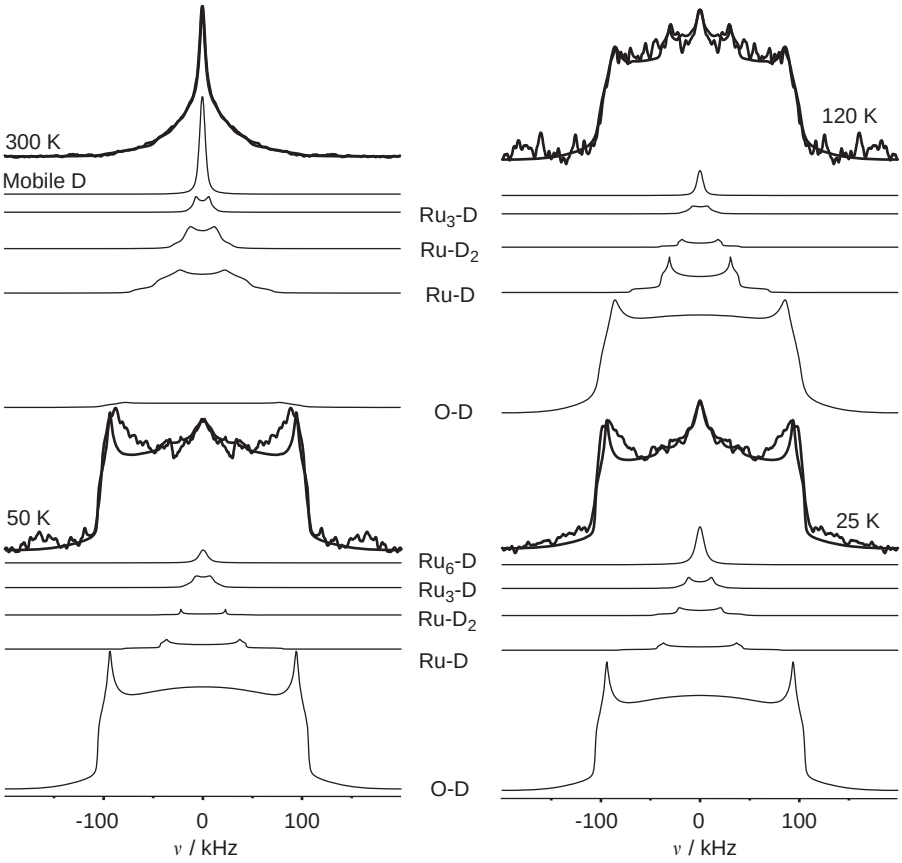

Fig. 3. Solid-state 46.03 MHz ^{2}H-NMR spectra of sample 2. The experimental spectra are simulated by the sum of the corresponding sub-spectra (see Table 2 and text).

Table 2
Parameters found by the line-shape analysis of ^{2}H-NMR spectra of Sample 2 (i.e. Q_{zz}, η, intensities, and the assignments of the signals).

T (K)	Signals	Intensities	Q_{zz} (kHz)	η	Assignments
300	Q_{zz1}	8.39×10^8	180	0.12	OD
	Q_{zz2}	1.4×10^9	70	0.35	RuD
	Q_{zz3}	6×10^8	30	0.2	RuD_2
	Q_{zz4}	2.15×10^8	14	0	Surface deuterium and/or Ru_3–D
120	Q_{zz1}	3.67×10^8	188	0.08	OD
	Q_{zz2}	2.24×10^7	70	0.12	RuD
	Q_{zz3}	3.21×10^6	40	0.1	RuD_2
	Q_{zz4}	2.6×10^6	18	0	Surface deuterium and/or Ru_3–D
50	Q_{zz1}	5.54×10^8	200	0.06	OD
	Q_{zz2}	9.5×10^6	80	0.08	RuD
	Q_{zz3}	1.44×10^6	45	0	RuD_2
	Q_{zz4}	5.2×10^6	18	0	Surface deuterium and/or Ru_3–D
25	Q_{zz1}	6.4×10^9	200	0.06	OD
	Q_{zz2}	9.44×10^6	80	0.08	RuD
	Q_{zz3}	7.52×10^6	45	0	RuD_2
	Q_{zz4}	6.57×10^6	24	0	Surface deuterium and/or Ru_3–D

the following quadrupolar parameters: $Q_{zz2} = 80$ kHz; $Q_{zz3} = 45$ kHz; $Q_{zz4} = 24$ kHz.

The component of 80 kHz can be attributed to deuterium atoms bound on top of a ruthenium atom. The component of 45 kHz is again tentatively attributed to fast rotating D_2 ligands. The narrow Pake-like line (Q_{zz4}) is attributed to threefold coordinated deuterium atoms, which are involved in the surface diffusion at higher than 25 K temperatures [59]. The broad component of 180–200 kHz can be attributed to O–D groups from deuterated Si–O–D groups of silica material. The dynamic line-shape changes between 120 and 300 K, resulting in the strong isotropic peak in the 300 K spectrum are an indication of a high mobility of the –Si–OD groups. The appearance of the narrow line at the 25 K spectrum can have two possible explanations, which are not mutually exclusive. Firstly, gaseous deuterium condenses to small micro-droplets. Secondly, deuterium atoms are coordinated inside Ru_6 octahedrons in the metallic ruthenium [59].

3.3. ^{2}H solid-state NMR studies of sample 3

$HO_2C(CH_2)_3SiO_{1.5}/9SiO_2$ was used as template for ruthenium nanoparticles (see Fig. 4). The pores of this mesoporous material have a diameter of 72 Å. While some of the particles agglomerated outside the material forming bigger clusters, the majority of the metal atoms formed the desired metal nanoparticles inside the silica. The incorporation of the particles in the pores is not very regular. Their average size was obtained by XRD analysis to be around 2.4 nm.

The low-temperature ^{2}H solid-state NMR measurements were performed in the temperature range of 50–300 K (see Fig. 5, Table 3). At room temperature the spectrum consists of five Pake-like sub-spectra and the narrow central line. The experimental values of the quadrupolar interaction for the five sub-spectra at room temperature are as follows: $Q_{zz1} = 160$ kHz; $Q_{zz2} = 130$ kHz; $Q_{zz3} = 70$ kHz; $Q_{zz4} = 40$ kHz; and $Q_{zz5} = 16$ kHz. Lowering the temperature goes in parallel with an increase of the intensities of the broad components. The 200 K spectrum can be decomposed into five Pake-like sub-spectra and a weak narrow line. The values of the quadrupolar interaction, found by line-shape analysis, give the quadrupolar parameters: $Q_{zz1} = 170$ kHz;

$Q_{zz2} = 130$ kHz; $Q_{zz3} = 80$ kHz; $Q_{zz4} = 40$ kHz; and $Q_{zz5} = 20$ kHz. The 80 K spectrum consists of five Pake-like sub-spectra with the Q_{zz} values of $Q_{zz1} = 174$ kHz; $Q_{zz2} = 130$ kHz; $Q_{zz3} = 76$ kHz; $Q_{zz4} = 36$ kHz; and $Q_{zz5} = 14$ kHz. At the lowest measured temperature (50 K) the spectrum consists of four Pake-like sub-spectra with the quadrupolar tensor values of $Q_{zz1} = 176$ kHz; $Q_{zz2} = 130$ kHz; $Q_{zz3} = 80$ kHz; $Q_{zz4} = 36$ kHz.

By virtue of the strength of the quadrupolar coupling, the 160–176 kHz line, which is characteristic of –OD, is attributed to surface Si–O–D groups of the silica and the 160–176 kHz line, which is characteristic of –CD, is attributed to partially deuterated carbons of $HO_2C(CH_2)_3SiO$ groups. From the preparation of the sample it is evident that no deuterons beyond the natural background of ca. 1% can be present inside the Ru at silica sample and that the D_2 gas is the only source of deuterium inside the sample. The heat of adsorption of hydrogen on pure silica is too low to activate the D_2 gas [61] and permit a deuteration of –SiOH or –CH2 groups. Thus the appearance of the broad components with 160–176 kHz and 130 kHz clearly shows the catalytic activity of the ruthenium nanoparticles.

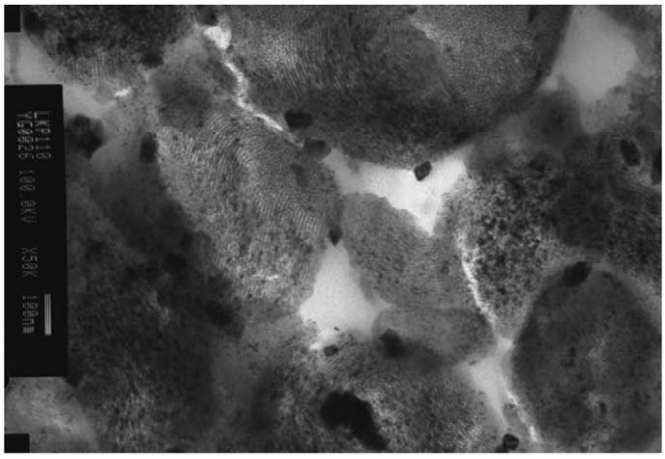

Fig. 4. TEM micrograph of ruthenium particles incorporated in $HO_2C(CH_2)3SiO1.5/9SiO_2$ [52].

The two remaining Pake-like sub-spectra are attributed to deuterium bound directly to ruthenium surface atoms. The Pake-like sub-spectrum with a Q_{zz} value of 70–80 kHz is characteristic of hydride like Ru–D deuterium bound on top of a ruthenium atom. Again there is a high mobility of the –SiOD groups at room temperature. The Pake-like sub-spectrum with 40 kHz is again tentatively attributed to dihydrogen like $Ru–D_2$ ligands, which are in fast rotational or tunneling exchange, which causes a characteristic reduction of the quadrupolar tensor. There also exists a possibility of physisorbed species on the nanoparticles surface, which would explain the narrowest component of 14–20 kHz in the spectra. However, this line might also be attributed to deuterium in the three-fold symmetry of ruthenium atoms, which is involved in the diffusion on the particles surface at higher temperatures, similar to sample 2 above.

3.4. Discussion

A major problem with the ^2H solid-state NMR of the nanoparticles inside silica was the deuteration of silanol (Si–OD) groups resulting in spectra with additional broad lines having high intensity and the characteristic quadrupolar coupling constant of an –Si–OD group. The mobility of these groups depends strongly on the sample preparation, which is evident by

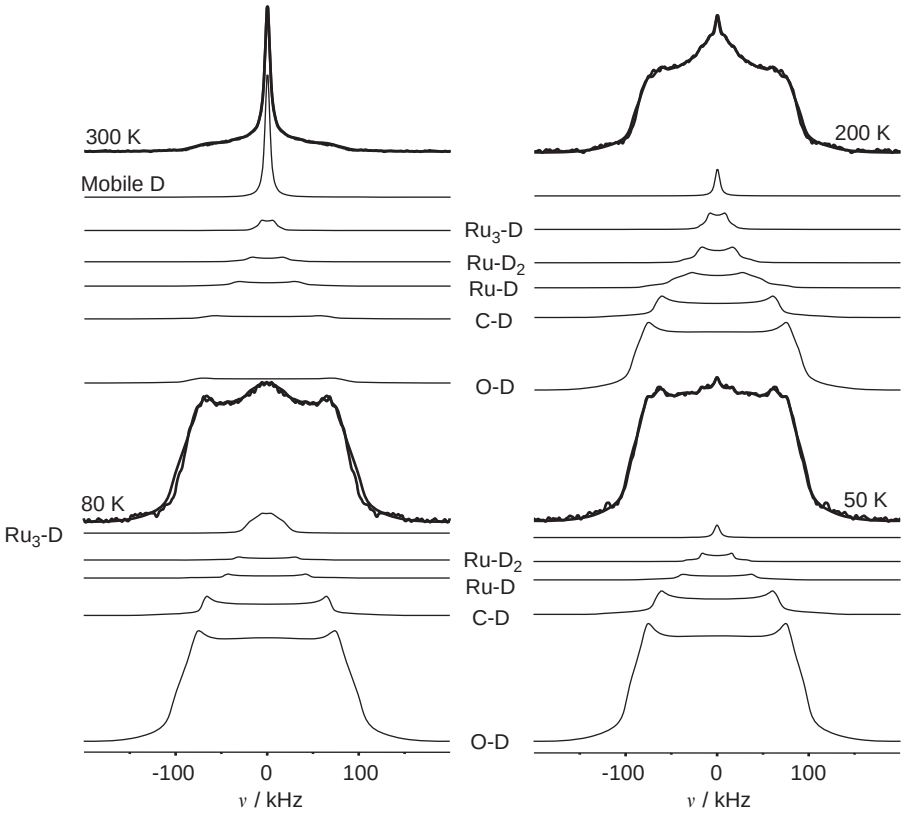

Fig. 5. Solid-state 46.03 MHz ^2H-NMR spectra of sample 3. The experimental spectra are simulated by the sum of the corresponding sub-spectra (see Table 3 and text).

Table 3
Parameters found by the line-shape analysis of ^{2}H-NMR spectra of Sample 3 (i.e. Q_{zz}, η, intensities, and the assignments of the signals).

T (K)	Signals	Intensities	$Q_{zz}\pm5$ (kHz)	$\eta\pm0.01$	Assignments
300	Q_{zz1}	2.24×10^9	160	0.10	OD
	Q_{zz2}	1.06×10^9	130	0.10	CD
	Q_{zz3}	8.32×10^8	70	0.10	RuD
	Q_{zz4}	4.83×10^8	40	0.15	RuD_2
	Q_{zz5}	5.25×10^8	16	0.10	Surface deuterium and/or Ru_3–D
200	Q_{zz1}	9.67×10^9	170	0.10	OD
	Q_{zz2}	1.78×10^9	130	0.06	CD
	Q_{zz3}	9.53×10^8	80	0.30	RuD
	Q_{zz4}	4.83×10^8	40	0.15	RuD_2
	Q_{zz5}	2.87×10^8	20	0.10	Surface deuterium and/or Ru_3–D
80	Q_{zz1}	2.46×10^9	174	0.13	OD
	Q_{zz2}	3×10^8	130	0.06	CD
	Q_{zz3}	5.26×10^7	76	0	RuD
	Q_{zz4}	4.45×10^7	36	0.20	RuD_2
	Q_{zz5}	2.66×10^7	14	0.30	Surface deuterium and/or Ru_3–D
50	Q_{zz1}	3.09×10^9	176	0.13	OD
	Q_{zz2}	3.35×10^8	130	0.06	CD
	Q_{zz3}	5.19×10^7	80	0	RuD
	Q_{zz4}	3.3×10^7	36	0	RuD_2

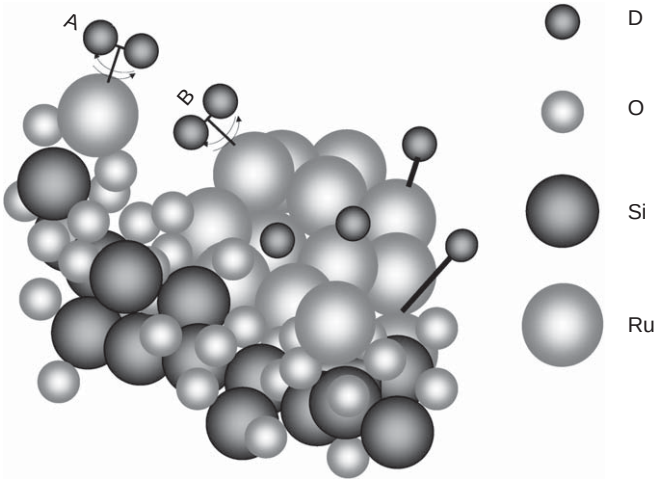

Fig. 6. Model of deuterium–ruthenium bonding situations on the nanopaticles caged by the mesoporous silica materials. While most of the deuterons are dissociated on the surface, forming different type of metal hydrides with varying bond length, there is also evidence for mobile deuterons, which are attributed to fast rotating Ru–D_2 ligands located at defects (A, B).

comparing the room temperature spectra of sample 1 to those of samples 2 and 3.

Compared to the intensity of the silanol groups, the signal of the deuterium bound to ruthenium appears in the spectra as small intensity Pake-like sub-spectra. Nevertheless, the quadrupolar splitting of these deuterium species were successfully revealed by line-shape analysis and attributed to the three bonding situations from the D–Ru bonding situation model.

From the results of the line-shape analysis a schematic model of the deuterium–ruthenium binding situations of ruthenium nanoparticles synthesized inside mesoporous materials can be made (see Fig. 6). In this model, besides the –OD deuterons, which are not shown for clarity, two types of deuterium atoms appear, namely hydride type deuterons (bound on top) and dihydrogen type deuterons. The deuterium bound on top of ruthenium atoms exhibits quadrupolar tensor values of 56–90 kHz. This shows that the bond distances play a crucial role here. In the first sample the two Pake-like sub-spectra with the Q_{zz} values of 56 and 90 kHz can be observed. The nanoparticles caged inside the SBA–3 might have two kinds of surface atoms exposed for deuterium atoms. One kind leads to a longer than 1.7 Å bond distance and the other leads to a shorter bond distance, respectively. Similar differences of Me–H bond lengths for hydrogen adsorbed at different sites of metal surfaces were found previously for other metal surfaces [62,63]. The Pake-like sub-spectra with quadrupolar splitting of 18–24 kHz, visible at temperatures below 50 K, are attributed to deuterium atoms which are coordinated to three ruthenium atoms in a three-fold symmetric site on the surface.

The question now arises about the origin of the weaker quadrupolar interaction with Q_{zz} values between 36 and 45 kHz. By comparison to studies of molecular Ru complexes we did tentatively attribute these signals to Ru–D_2 ligands. In principle there are two different possible origins of such ligands, namely (A) isolated Ru-atoms or molecular complexes on the surface and (B) metallic Ru-parts on the surface. The second case would necessitate the presence of hydrogen, which is nondissociatively chemisorbed on the metal surface. Calculations by Norskov et al. [64] and van Santen et al. [63] give typical dissociation energies of ca. 100 kJ/mol for molecular hydrogen on a Ru surface at low (sub-monomolecular) coverage. This energy difference shifts the dissociation equilibrium strongly to the dissociated state. However, the calculations reveal also the existence of metal sites with lower dissociation energies of 18 kJ/mol [63]. Ertl et al. [65] have reported the existence of dihydrogen on RuO surfaces and calculated the corresponding distance between the H_2 ligand and the ruthenium atom on the surface of $RuO_2(1\,1\,0)$ as 1.8 Å, and the H–H bond length ≈0.89 Å. These results coincide with the bond lengths in η^2–H_2 complexes, and also with the Ru–D and D–D bond distances in our investigated ruthenium model complexes [34]. This corroborates our tentative attribution of the Q_{zz} values between 36 and 45 kHz in to D_2 ligands. Moreover, one can conclude that these dihydrogen ligands are either bound to Ru-atoms, isolated on the surface, which behave like a ruthenium oxide type or that they are bound to special defect sites on the metal. In both cases they have the high rotational mobility which is characteristic of dihydrogen ligands.

4. Summary and conclusions

A set of three different catalytically active ruthenium coated mesoporous silica materials was studied by variable temperature ^{2}H-solid-state NMR line-shape analysis. Comparing the data of this line-shape analysis with reference data from model complexes, it is possible to reveal the different deuteron species insides of the samples. In all samples a strong –OD signal is found, which shows the catalytic activity of the metal, which activates the D–D bond and deuterates the –SiOH groups. In addition the presence of different types of deuterons, bound to the metal is revealed. The singly coordinated –Ru–D species exhibit several different quadrupolar couplings, which indicate the presence of several non-equivalent binding sites with differing binding strength. The dihydrogen species –Ru–D_2 which is attributed to surface defects, exhibits a fast rotational dynamics at all temperatures.

Thus, it is shown that the deuteron quadrupolar interaction can be employed for the characterization of systems with unknown deuteron binding situations and ^{2}H solid-state NMR techniques indeed provide the means for a deep characterization of the behavior of hydrogen interacting with a metal surface and can thus give new and interesting insights into basic catalytic mechanisms as in particular hydrogenation reactions.

Acknowledgments

Financial support by the Deutsche Forschungsgemeinschaft under contract Bu 911/12-1 is gratefully acknowledged. Jianlin Huang thanks the Sino-German program of the NSFC and the DFG for a stipend under contract CHV-113-262-0-1.We thank the group of Dr. Bruno Chaudret at the Laboratoire de Chimie de Coordination du CNRS, Toulouse, for the donation of one of the Ru/silica samples.

References

[1] H. Brunner, E. Bielmeier, J. Wiehl, J. Organomet. Chem. 384 (1990) 223–241.
[2] B.E. Handy, I. Gorzkowska, J. Nickl, A. Baiker, M. Schramlmarth, A. Wokaun, Ber. Bunsen Phys. Chem. 96 (1992) 1832–1840.
[3] H. Werner, U. Mohring, J. Organomet. Chem. 475 (1994) 277–282.
[4] J. Bluemel, Ber. Bunsen Phys. Chem. 99 (1995) 1343–1346.
[5] D. Brunel, N. Bellocq, P. Sutra, A. Cauvel, M. Lasperas, P. Moreau, F. Di Renzo, A. Galarneau, F. Fajula, Coord. Chem. Rev. 180 (1998) 1085–1108.
[6] J. Evans, A.B. Zaki, M.Y. El-Sheikh, S.A. El-Safty, J. Phys. Chem. B 104 (2000) 10271–10281.
[7] C. Merckle, S. Haubrich, J. Bluemel, J. Organomet. Chem. 627 (2001) 44–54.
[8] A.J. Sandee, J.N.H. Reek, P.C.J. Kamer, P.W.N.M. van Leeuwen, J. Am. Chem. Soc. 123 (2001) 8468–8476.
[9] W.H. Cheung, W.Y. Yu, W.P. Yip, N.Y. Zhu, C.M. Che, J. Org. Chem. 67 (2002) 7716–7723.
[10] T. Joseph, S.S. Deshpande, S.B. Halligudi, A. Vinu, S. Ernst, M. Hartmann, J. Mol. Catal. A Chem. 206 (2003) 13–21.
[11] H.L. Li, N. Perkas, Q.L. Li, Y. Gofer, Y. Koltypin, A. Gedanken, Langmuir 19 (2003) 10409–10413.
[12] J.O. Krause, O. Nuyken, K. Wurst, M.R. Buchmeiser, Chem. Eur. J. 10 (2004) 777–784.
[13] M.W. McKittrick, C.W. Jones, J. Catal. 227 (2004) 186–201.
[14] S. Shylesh, A.P. Singh, J. Catal. 228 (2004) 333–346.
[15] A. Crosman, W.E. Hoelderich, J. Catal. 232 (2005) 43–50.
[16] C. Merckle, J. Bluemel, Top. Catal. 34 (2005) 5–15.
[17] N.K.K. Raj, S.S. Deshpande, R.H. Ingle, T. Raja, P. Manikandan, Nanoporous Mater. IV 156 (2005) 769–778.
[18] P.M. Rao, A. Wolfson, S. Kababya, S. Vega, M.V. Landau, J. Catal. 232 (2005) 210–225.
[19] A.M.J. Rost, H. Schneider, J.P. Zoller, W.A. Herrmann, F.E. Kuhn, J. Organomet. Chem. 690 (2005) 4712–4718.
[20] J. Bluemel, Nachr. Chem. 54 (2006) 632–638.
[21] M. Hartmann, C. Streb, J. Porous. Mat. 13 (2006) 347–352.
[22] J. Kasai, Y. Nakagawa, S. Uchida, K. Yamaguchi, N. Mizuno, Chem. Eur. J. 12 (2006) 4176–4184.
[23] T. Posset, J. Bluemel, J. Am. Chem. Soc. 128 (2006) 8394–8395.
[24] S. Hermes, M. Schroter, R. Schmid, L. Khodeir, M. Muhler, A. Tissler, R. Fischer, R. Fischer, Angew. Chem. Int. Ed. 44 (2005) 6237–6241.
[25] F. Hoffmann, M. Cornelius, J. Morell, M. Froba, Angew. Chem. Int. Ed. 45 (2006) 3216–3251.
[26] X.S. Zhao, X.Y. Bao, W. Guo, F.Y. Lee, Mater. Today 9 (2006) 32–39.
[27] M. Heitbaum, F. Glorius, I. Escher, Angew. Chem. Int. Ed. 45 (2006) 4732–4762.
[28] G. Buntkowsky, H.H. Limbach, F. Wehrmann, I. Sack, H.M. Vieth, R.H. Morris, J. Phys. Chem. A 101 (1997) 4679.
[29] F. Wehrmann, T. Fong, R.H. Morris, H.H. Limbach, G. Buntkowsky, Phys. Chem. Chem. Phys. 1 (1999) 4033.
[30] F. Wehrmann, J. Albrecht, E. Gedat, G.J. Kubas, H.H. Limbach, G. Buntkowsky, J. Phys. Chem. A 106 (2002) 2855.
[31] G. Buntkowsky, B. Walaszek, A. Adamczyk, Y. Xu, H.H. Limbach, B. Chaudret, Phys. Chem. Chem. Phys. 8 (2006) 1929–1935.
[32] F. Schröder, D. Esken, M. Cokoja, M.W.E.v.d. Berg, O. Lebedev, G.V. Tendeloo, B. Walaszek, G. Buntkowsky, H.H. Limbach, B. Chaudret, R.A. Fischer, J.Am. Chem. Soc. 130 (2008) 6119–6130.
[33] A. Adamczyk, Y. Xu, B. Walaszek, F. Roelofs, T. Pery, K. Pelzer, K. Philippot, B. Chaudret, H.H. Limbach, H. Breitzke, G. Buntkowsky, Top. Catal. 48 (2008) 75–83.
[34] B. Walaszek, A. Adamczyk, T. Pery, X. Yeping, T. Gutmann, N. Amadeu de Sousa, S. Ulrich, H. Breitzke, H.M. Vieth, S. Sabo-Etienne, B. Chaudret, H.H. Limbach, G. Buntkowsky, J. Am. Chem. Soc. 130 (2008) 17502–17508.
[35] T. Pery, K. Pelzer, G. Buntkowsky, K. Philippot, H.H. Limbach, B. Chaudret, Chem. Phys. Chem. 6 (2005) 605.
[36] J.S. Beck, J.C. Vartuli, W.J. Roth, M.E. Leonowicz, C.T. Kresge, K.D. Schmitt, C.T.W. Chu, D.H. Olson, E.W. Sheppard, S.B. Mccullen, J.B. Higgins, J.L. Schlenker, J. Am. Chem. Soc. 114 (1992) 10834–10843.
[37] A. Corma, Chem. Rev. 97 (1997) 2373–2419.
[38] M. Vallet-Regi, F. Balas, D. Arcos, Angew. Chem. Int. Ed. 46 (2007) 7548–7558.
[39] L.F. Giraldo, B.L. Lopez, L. Perez, S. Urrego, L. Sierra, M. Mesa, Macromol. Symp. 258 (2007) 129–141.
[40] C.Y. Mou, H.P. Lin, Pure Appl. Chem. 72 (2000) 137–146.
[41] S.A. Bagshaw, E. Prouzet, T.J. Pinnavaia, Science 269 (1995) 1242–1244.
[42] D.Y. Zhao, Q.S. Huo, J.L. Feng, B.F. Chmelka, G.D. Stucky, J. Am. Chem. Soc. 120 (1998) 6024–6036.
[43] Y.P. Xu, S.J. Xu, T. Emmler, F. Roelofs, C. Boettcher, R. Haag, G. Buntkowsky, Chem. Eur. J. 14 (2008) 3311–3315.
[44] N.T. Whilton, B. Berton, L. Bronstein, H.P. Hentze, M. Antonietti, Adv. Mater. 11 (1999) 1014–1018.
[45] X. Feng, G.E. Fryxell, L.Q. Wang, A.Y. Kim, J. Liu, K.M. Kemner, Science 276 (1997) 923–926.
[46] C. Zapilko, M. Widenmeyer, I. Nagl, F. Estler, R. Anwander, G. Raudaschl-Sieber, O. Groeger, G. Engelhardt, J. Am. Chem. Soc. 128 (2006) 16266–16276.
[47] K. Moller, T. Bein, Chem. Mater. 10 (1998) 2950–2963.
[48] A. Vyalikh, T. Emmler, I. Shenderovich, Y. Zeng, G.H. Findenegg, G. Buntkowsky, Phys. Chem. Chem. Phys. 9 (2007) 2249–2257.
[49] B.A. Riguetto, C.E.C. Rodrigues, M.A. Morales, E. Baggio-Saitovitch, L. Gengembre, E. Payen, C.M.P. Marques, J.M.C. Bueno, Appl. Catal. A Gen. 318 (2007) 70–78.
[50] M. Nurunnabi, K. Murata, K. Okabe, M. Inaba, I. Takahara, Appl. Catal. A Gen. 340 (2008) 203–211.
[51] E.P. Barrett, L.G. Joyner, P.P. Halenda, J. Am. Chem. Soc. 73 (1951) 373.
[52] K. Pelzer, Dissertation UGH Essen, 2003.
[53] K. Schmidt-Rohr, H.W. Spiess, Multidimensional Solid State NMR and Polymers, Academic Press, London, 1994.
[54] G. Buntkowsky, M. Taupitz, E. Roessler, H.M. Vieth, J. Phys. Chem. A 101 (1997) 67.
[55] E. Gedat, A. Schreiber, J. Albrecht, I. Shenderovich, G. Findenegg, H.H. Limbach, G. Buntkowsky, J. Phys. Chem. B. 106 (2002) 1977.
[56] W. Masierak, T. Emmler, E. Gedat, A. Schreiber, G.H. Findenegg, G. Buntkowsky, J. Phys. Chem. B (2004) 18890–18896.
[57] G. Buntkowsky, H.H. Limbach, in: J.P. Hynes, J.P. Klinman, H.H. Limbach, R.L. Schowen (Eds.), Hydrogen-Transfer Reactions, vol. 2, Wiley-VCH, Weinheim, 2006, pp. 639–682.
[58] G. Buntkowsky, H.H. Limbach, J. Low. Temp. Phys. 143 (2006) 55–114.
[59] B. Walaszek, T. Gutmann, Y. Xu, M. Wächtler, A. Adamczyk, I.d. Rosal, R. Poteau, R. Axet, G. Lavigne, B. Chaudret, H.-H. Limbach, G. Buntkowsky, 2009, in preparation.
[60] T.M. Clark, P.J. Grandinetti, J Phys. Condens. Matter 15 (2003) S2387–S2395.
[61] K.J. Edler, P.A. Reynolds, P.J. Branton, F.R. Trouw, J.W. White, J. Chem. Soc. Faraday Trans. 93 (1997) 1667–1674.
[62] R. Doell, L. Hammer, K. Heinz, K. Bedurftig, U. Muschiol, K. Christmann, A.P. Seitsonen, H. Bludau, H. Over, J. Chem. Phys. 108 (1998) 8671–8679.
[63] I.M. Ciobica, A.W. Kleyn, R.A. Van Santen, J. Phys. Chem. B 107 (2003) 164–172.
[64] T.H. Rod, A. Logadottir, J.K. Norskov, J. Chem. Phys. 112 (2000) 5343–5347.
[65] J.H. Wang, C.Y. Fan, Q. Sun, K. Reuter, K. Jacobi, M. Scheffler, G. Ertl, Angew. Chem. Int. Ed. 42 (2003) 2151–2154.